Materials Today Energy 26 (2022) 100983

Contents lists available at ScienceDirect

Materials Today Energy

journal homepage: www.journals.elsevier.com/materials-today-energy/

Synergistically optimizing carrier and phonon transport properties in *n*-type PbTe through I doping and SnSe alloying

Wei Liu [a, b], Tao Hong [c], Shizhi Dong [b], Dongyang Wang [c], Xiang Gao [d], Yu Xiao [a, *], Li-Dong Zhao [c, **]

[a] State Key Laboratory for Mechanical Behavior of Materials, Xi'an Jiaotong University, Xi'an, 710049, China
[b] College of Materials Science and Engineering, Liaoning Technical University, Fuxin, 123000, China
[c] School of Materials Science and Engineering, Beihang University, Beijing, 100191, China
[d] Center for High Pressure Science and Technology Advanced Research (HPSTAR), Beijing, 100094, China

ARTICLE INFO

Article history:
Received 20 January 2022
Received in revised form
24 February 2022
Accepted 1 March 2022
Available online 7 March 2022

Keywords:
Thermoelectric material
Carrier mobility
Thermal conductivity
ZT value

ABSTRACT

PbTe is a promising thermoelectric material, but the properties in *n*-type PbTe need further improvement to match its advanced *p*-type material. In this work, the thermoelectric performance in *n*-type PbTe is synergistically enhanced with iodine (I) doping and SnSe alloying. The experiments show that I element is a good donor dopant to tune the carrier density and SnSe alloying can effectively balance the triple-relations between carrier mobility, carrier effective mass, and lattice thermal conductivity. Thus, high carrier mobility of ~755 $cm^2V^{-1}s^{-1}$ results in an optimum power factor (*PF*) of ~27.0 $\mu Wcm^{-1}K^{-2}$ in PbTe −2%SnSe at 573 K. Microstructure observation reveals the dispersively embedded Sn-rich nano-precipitates in PbTe−2%SnSe, which largely suppresses lattice thermal conductivity at room temperature, from ~3.41 $Wm^{-1}K^{-1}$ in PbTe to ~1.01 $Wm^{-1}K^{-1}$ in PbTe−2%SnSe. Combined the optimized *PF* and decreased thermal conductivity, the peak *ZT* value of ~1.5 can be obtained at 773 K in PbTe−2%SnSe. The obtained high thermoelectric performance in our work is comparable with other advanced *n*-type PbTe thermoelectrics and has great application potential.

1. Introduction

Thermoelectric technology provides an alternative way to relieve the increasing environmental deterioration and energy crisis. According to Seebeck effect, waste heat is converted directly into electric energy by thermoelectric materials [1–5], which could effectively alleviate the cumulatively environmental crisis and severe energy. Thermoelectric performance is determined by a dimensionless figure of merit *ZT*, $ZT = (\sigma S^2 T)/\kappa_{tot}$, where *S*, σ, κ_{tot}, and *T* refer to Seebeck coefficient, electrical conductivity, total thermal conductivity, and temperature in Kelvin, respectively [6–9]. Obviously, excellent thermoelectric material simultaneously demands prominent *PF* ($PF = S^2\sigma$) and low total thermal conductivity [10–13], which is the sum of electronic thermal conductivity (κ_{ele}) and lattice thermal conductivity (κ_{lat}). However, these coupling relations between thermoelectric parameters make it difficult to improve final *ZT* value.

Among these advanced thermoelectric materials, PbTe is one of typical thermoelectric candidates at intermediate temperature [14,15]. However, the comparably low *ZT* value in *n*-type PbTe is the main obstacle to the widespread popularization of PbTe-based material. Hence, it is urgent to improve the performance in *n*-type PbTe so as to match its advanced *p*-type system. To date, strategies to optimize the thermoelectric efficiency in *n*-type PbTe mainly include *PF* optimization and thermal conductivity reduction. The strategies to improve *PF* mainly include doping to optimize carrier density [16–20], electronic band structure manipulation to optimize carrier effective mass [21–23]. To reduce thermal conductivity, all-scale defect structure designing is widely applied, such as point defect [24,25], dislocation [26,27], nanoprecipitate, [28,29], grain boundary [30–32], *etc*. However, the strongly coupled electrical and thermal transport properties make these strategies difficult to achieve much enhancement in the final *ZT* value. In order to maximize the thermoelectric performance in *n*-type PbTe, it is important to synergistically regulate the carrier and phonon transport.

In this work, I element is selected to tune the carrier density in PbTe and contributes to an optimal *PF* of ~25.5 $\mu Wcm^{-1}K^{-2}$ in *n*-type

* Corresponding author.
** Corresponding author.
E-mail addresses: xiao_yu@xjtu.edu.cn (Y. Xiao), zhaolidong@buaa.edu.cn (L.-D. Zhao).

https://doi.org/10.1016/j.mtener.2022.100983
2468-6069/

$PbTe_{0.995}I_{0.005}$ at 573 K. Based on the optimal carrier density in *n*-type PbTe ($PbTe_{0.995}I_{0.004}$), SnSe alloying is further conducted in PbTe, which successfully regulated the coupling relations between effective mass and carrier mobility due to band sharpening. The room temperature carrier mobility increases from ~325 $cm^{-2}V^{-1}s^{-1}$ in *n*-type PbTe to ~755 $cm^{-2}V^{-1}s^{-1}$ in PbTe−2%SnSe. Besides, microstructure observation reveals that PbTe−2%SnSe sample includes massive Sn-rich nanoprecipitates, which largely suppresses the lattice thermal conductivity to ~1.01 $Wm^{-1}K^{-1}$ in PbTe−2%SnSe at 300 K. As a result, these regulation of carrier and phonon transport behaviors in PbTe−2%SnSe samples benefit a remarkable improvement in the quality factor (B) at 300−773 K, and a peak ZT of ~1.5 can be obtained in *n*-type PbTe−2%SnSe.

2. Experimental details

The PbTe materials in our work were synthesized through melting reaction and spark plasma sintering to gain dense samples. The phase was identified by X-ray diffraction. The microstructure was studied by (scanning) transmission electron microscopy (SEM and TEM) and energy-dispersive X-ray spectroscopy (EDS). The electrical transport properties were measured using Cryoall CTA. Thermal diffusivity was acquired with Netzsch LFA457. The heat capacity was obtained by Debye model [33]. More experimental details of thermoelectric performance measurements, phases, and microstructure in this work are given in the Supporting Information (SI).

3. Results and discussion

To synergistically improve the electrical and thermal transport properties in *n*-type PbTe, this work introduces I doping and SnSe alloying as following steps. First, the *n*-type PbTe is achieved by I doping to optimize its carrier density. Second, based on the optimized carrier density in $PbTe_{0.995}I_{0.004}$, SnSe alloying is introduced to regulate the coupling relations between carrier effective mass

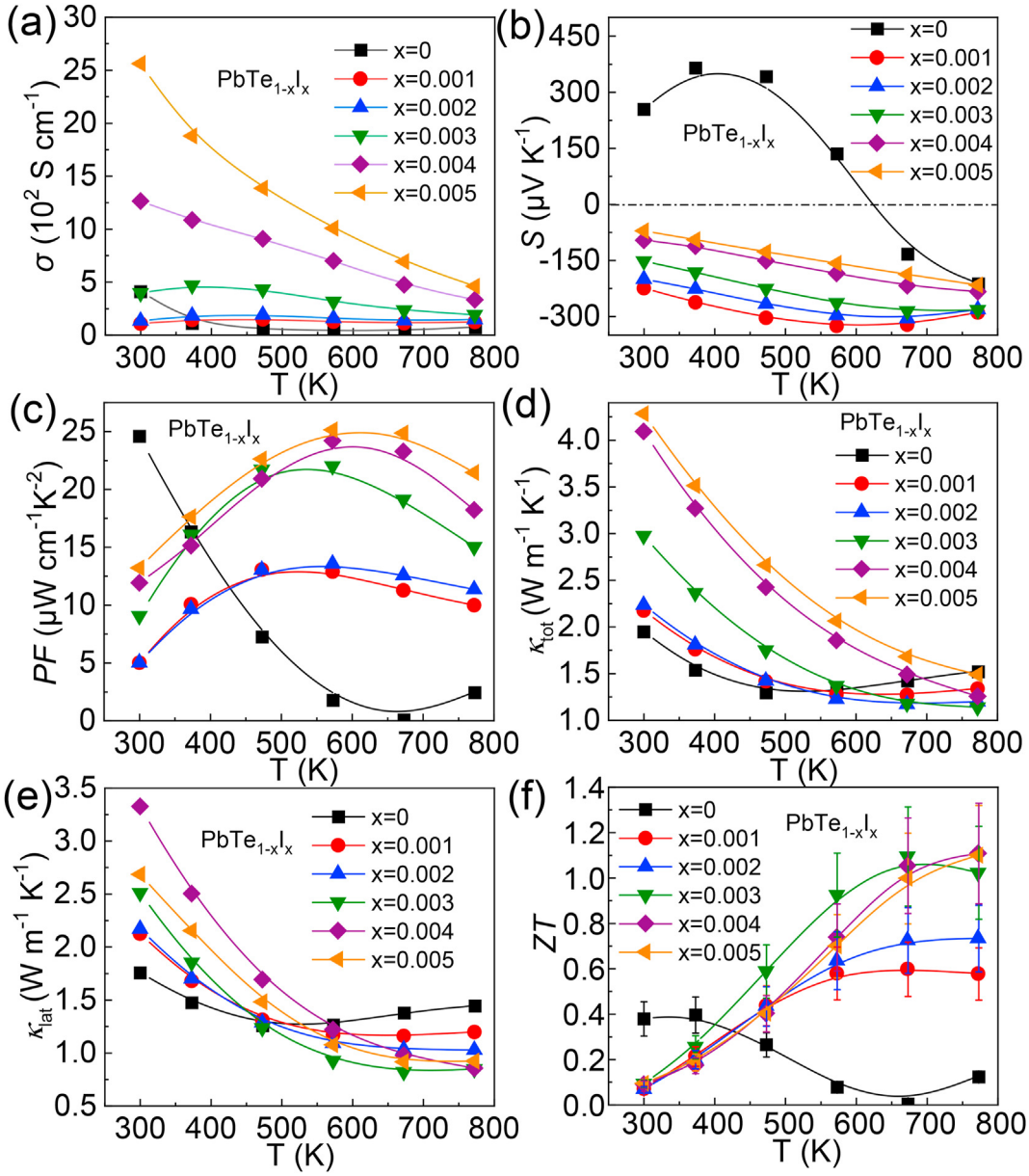

Fig. 1. Thermoelectric properties of $PbTe_{1-x}I_x$ (x=0−0.005): (a) electrical conductivity; (b) Seebeck coefficient; (c) power factor; (d) total thermal conductivity; (e) lattice thermal conductivity; (f) ZT value.

and carrier mobility, thus obtain the improved electrical transport properties. Third, microstructure observation results elucidate the dispersive Sn-rich precipitates, which are the origins of low lattice thermal conductivity in PbTe−2%SnSe.

Thermoelectric transport performance in $PbTe_{1-x}I_x$ (x=0−0.005). Fig. S1(a) displays the XRD results of $PbTe_{1-x}I_x$ (x = 0−0.005) and no impurity phases are observed. And the evaluated lattice parameters in $PbTe_{1-x}I_x$ (x = 0−0.005) undergo a decreasing trend with increasing I doping content, show in Fig. S1(b), which indicates I atom was effectively introduced into Te site in PbTe matrix. Because of the enhanced carrier density in I-doped PbTe, the electrical conductivity of room temperature in Fig. 1(a) significantly increases from ~409 Scm^{-1} in PbTe to ~ 2562 Scm^{-1} in $PbTe_{0.995}I_{0.005}$. Correspondingly, all the I-doped PbTe samples present negative Seebeck coefficient in Fig. 1(b), and the optimized *PF* of ~25.5 $\mu Wcm^{-1}K^{-2}$ in $PbTe_{0.995}I_{0.005}$ at 573 K in Fig. 1(c). Besides, the total thermal conductivity in $PbTe_{1-x}I_x$ (x = 0−0.005) gets obvious increase after I doping in Fig. 1(d). The higher total thermal conductivity in $PbTe_{1-x}I_x$ (x = 0−0.005) arises from both increased electronic thermal conductivity and lattice thermal conductivity in Fig. S2(d) and Fig. 1(e). As a result, the optimum *ZT* value of ~1.1 can be achieved in $PbTe_{0.996}I_{0.004}$ at 773 K, as shown in Fig. 1(f). Additional details about thermal transport properties in $PbTe_{1-x}I_x$ (x = 0−0.005) can be found in Fig. S2.

Electrical performance in PbTe−y%SnSe (y=0−4). In this section, all the PbTe-based samples are continually optimized based on the composition of $PbTe_{0.996}I_{0.004}$. To short the sample name, the I doping content will not be mentioned in following discussion. The XRD results in PbTe−y%SnSe (y = 0−4) display that no impurity phase is observed in Fig. S3(a). Correspondingly, the calculated lattice parameter in PbTe−y%SnSe (y = 0−4) shows a linear decreasing trend with increasing SnSe content, shown in Fig. S3(b).

The electrical transport properties in PbTe−y%SnSe (y = 0−4) are showed in Fig. 2. After SnSe alloying, the electrical conductivity in PbTe−y%SnSe (y = 0−4) significantly increases in the entire

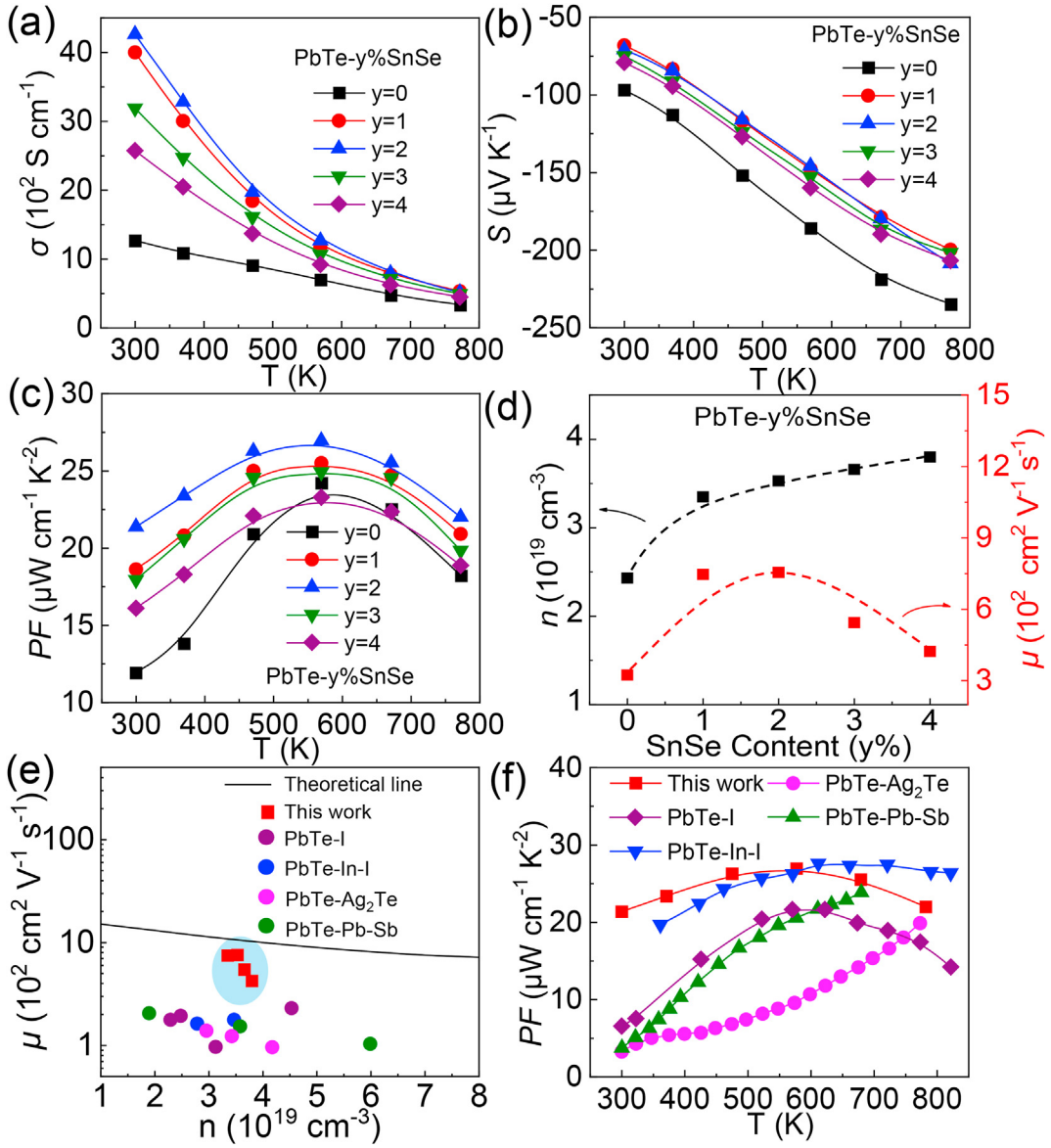

Fig. 2. Electrical transport properties of PbTe−y%SnSe (y = 0−4): (a) electrical conductivity; (b) Seebeck coefficient; (c) power factor; (d) carrier density and carrier mobility as a function of SnSe content; (e) carrier mobility as a function of carrier density and its comparison with other *n*-type PbTe-based samples: PbTe−I [34], PbTe−In−I [35], PbTe−Ag_2Te [36], PbTe−Pb−Sb [37]; (f) power factor.

temperature range, shown in Fig. 2(a). And the large increase of electrical transport properties in SnSe-alloyed PbTe originate from the changes of carrier density and carrier effective mass, which will be discussed below. From the Seebeck coefficient in Fig. 2(b), PbTe−y%SnSe (y = 0−4) present a slightly reduced absolute value of Seebeck coefficient after SnSe alloying. The significantly improved electrical conductivity and slightly decreased Seebeck coefficient in PbTe−y%SnSe (y = 0−4) largely improve the *PF*, and the optimum *PF* increases from ~24.2 μWcm^{-1}K^{-2} in PbTe to ~ 27.0 μWcm^{-1}K^{-2} in PbTe−2%SnSe in Fig. 2(c). The Hall measurement results in Fig. 2(d) and Table S1 show that the carrier density in PbTe−y%SnSe (y = 0−4) slightly increases with increasing SnSe alloying content, and the carrier mobility increases from ~325 cm^{-2}V^{-1}s^{-1} in PbTe to ~ 755 cm^{-2}V^{-1}s^{-1} in PbTe−2%SnSe at 300 K. Compared with some other *n*-type PbTe materials, the PbTe−y%SnSe (y = 0−4) samples present superior carrier mobility and *PF*, as shown in Fig. 2(e) and (f).

These enhanced electrical performance in PbTe−y%SnSe (y = 0−4) is closely related to the competing relations between carrier density, carrier mobility, and carrier effective mass. Therefore, the band structure is studied to further investigate its origins in enhanced electrical transport properties in SnSe-alloyed PbTe. In this work, the bandgap in PbTe−y%SnSe (y = 0−4) is reduced with increasing SnSe alloying fraction, from ~0.28 eV in PbTe to ~ 0.24 eV in PbTe−4%SnSe in Fig. 3(a). With narrowing bandgap, the conduction band shape in PbTe−y%SnSe (y = 0−4) become sharper with increasing SnSe alloying content, as depicted in Fig. 3(b). For a single electronic band structure, the carrier effective mass depends on the electronic band shape, and sharper band owns a lower carrier effective mass and vice versa [38−42]. From Pisarenko relation in Fig. 3(c), the carrier effective mass in PbTe is slightly reduced after SnSe alloying. Although the reduced carrier effective mass will deteriorate the Seebeck coefficient, the lower carrier effective mass is favorable for high carrier mobility. To evaluate the effect of SnSe alloying on carrier transport properties in PbTe−y%SnSe (y = 0−4), the temperature-dependent weighted mobility (μ_W) is presented in Fig. 3(d). The weighted mobility in SnSe-alloyed PbTe is significantly enhanced especially at 300−573 K, and the maximum weighted mobility increases from ~151 cm^{-2}V^{-1}s^{-1} in PbTe to ~346 cm^{-2}V^{-1}s^{-1} in PbTe−2%SnSe at 300 K. The obviously enhanced weighted mobility contributes to high *PF*, which originates from the balanced competitive relationships of carrier effective mass, carrier density, and carrier mobility.

Thermal transport properties and microstructure in PbTe−y%SnSe (y=0−4). The total thermal conductivity is largely reduced after SnSe alloying, as shown in Fig. 4(a). Noticeably, as a parameter that can be regulated independently, the lattice thermal conductivity significantly decreases from ~3.41 Wm^{-1}K^{-1} in PbTe to ~1.01 Wm^{-1}K^{-1} in PbTe−2%SnSe at 300 K in Fig. 4(b). More details about thermal transport properties in PbTe−y%SnSe (y = 0−4) can be found in Fig. S4. In order to further investigate the low lattice thermal conductivity in PbTe−y%SnSe (y = 0−4), ultrasonic measurement is conducted to evaluate the elastic properties based on the sound velocity data.

Table S2 presents the results of sound velocity in PbTe−y%SnSe (y = 0−4), which can be used to explore the origins of the reduced lattice thermal conductivity, which can be expressed as [43,44]:

$$\kappa_L = \frac{1}{3} C_V \nu_a l \tag{1}$$

$$l = \tau \nu_a \tag{2}$$

where C_v, ν_a, l, and τ denote the specific heat at constant volume, the phonon velocity, the phonon mean free path, and relaxation

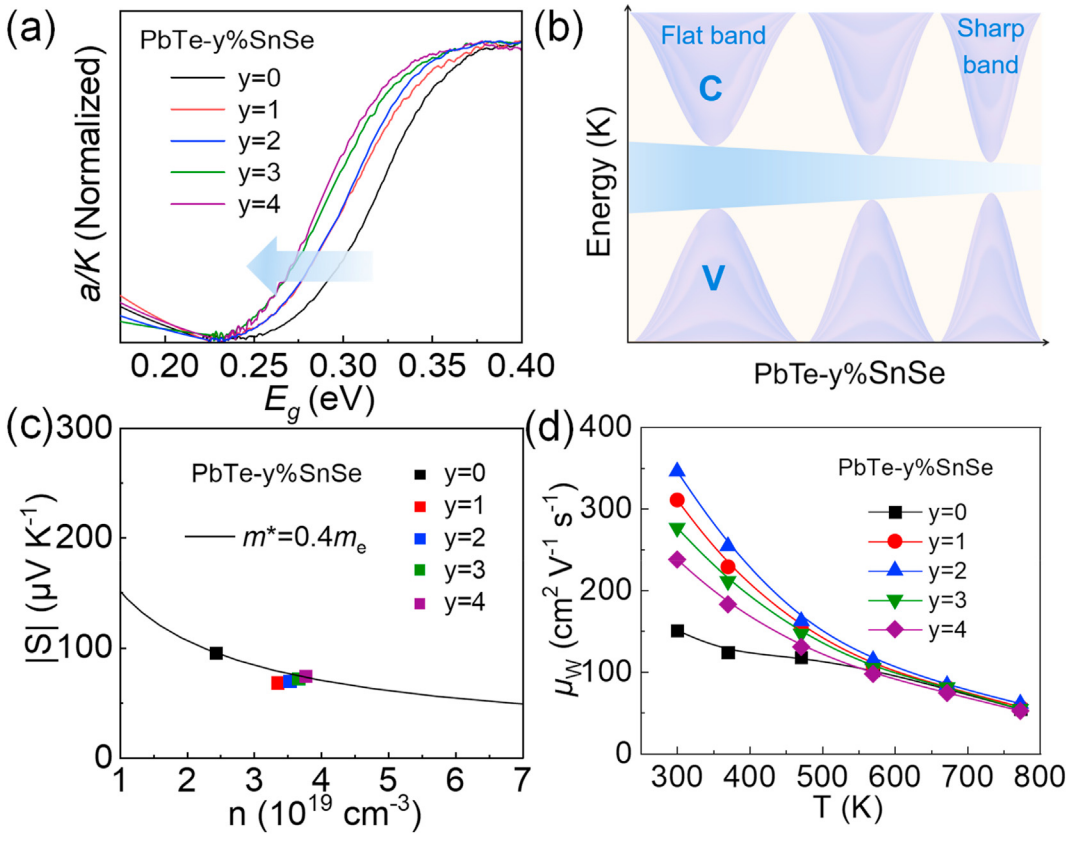

Fig. 3. Band structures of PbTe−y%SnSe (y = 0−4): (a) optical bandgap; (b) schematic of electronic band evolution; (c) Pisarenko relation; (d) weighted mobility.

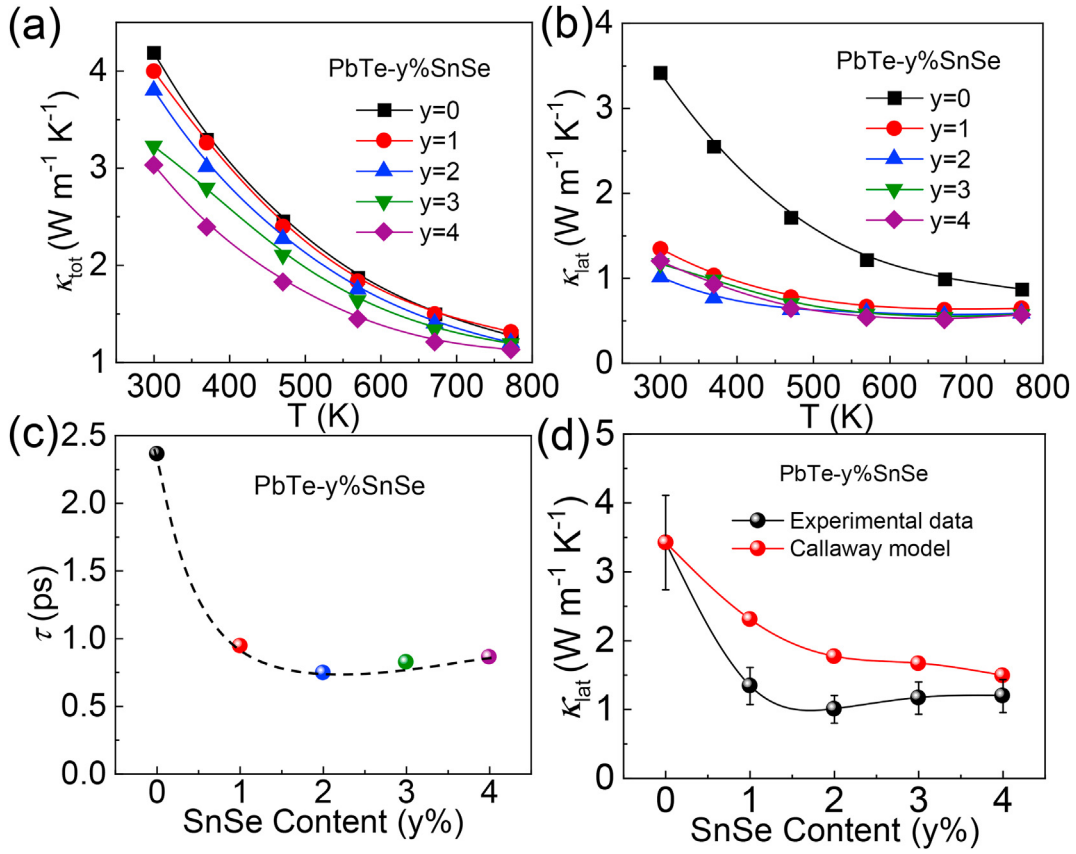

Fig. 4. Thermoelectric properties of PbTe−y%SnSe (y = 0–4): (a) total thermal conductivity; (b) lattice thermal conductivity; (c) phonon relaxation time as a function of SnSe content; (d) comparison of room temperature lattice thermal conductivity between experimental results and Callaway model estimations.

time, respectively. Here, v_a can be taken as the average of longitudinal (v_l) and transverse (v_t) velocities [45,46]. The experimental results show that SnSe alloying can greatly reduce the phonon relaxation time in *n*-type PbTe, from ~2.37 ps in PbTe to ~0.75 ps in PbTe−2%SnSe, as shown in Fig. 4(c). The reduced phonon relaxation time in SnSe-alloyed PbTe is due to intensified phonon scattering by imported defects.

According to the Callaway model, SnSe alloying in PbTe can import point defects and cause atomic size and mass fluctuations. The lattice thermal conductivity follows the relations [47–50]:

$$\frac{\kappa_{lat}}{\kappa_{lat,P}} = \frac{\tan^{-1}(u)}{u} \tag{3}$$

where $\kappa_{lat,p}$ is the lattice thermal conductivities in the parent material, and the parameter u is expressed as [47,48]:

$$u = \left(\frac{\pi^2 \theta_D \Omega}{h v_a^2} \kappa_{L,p} \Gamma\right)^{1/2} \tag{4}$$

where θ_D, Ω, Γ, h, and v_a stand for the Debye temperature, average volume per atom, imperfection scaling parameter, Planck constant and average sound velocity. The Γ includes two parts: Γ_M (mass fluctuation) and Γ_S (strain field fluctuation), and they follow the equation: $\Gamma = \Gamma_M + \varepsilon\Gamma_S$, where ε as a phenomenological adjustable parameter, the calculation details are show in eqs S4-S6. This work needs to consider Pb sites are substituted Sn atoms and Te sites are substituted Se atoms, which is represented by Refs. [48,51]:

$$\Gamma_{P_X Q_{1-X}} = \frac{1}{2}\left(\frac{M_{(P,Q)}}{\overline{M}}\right)^2 \Gamma_{(P,Q)} \tag{5}$$

$$\Gamma_{(P,Q)} = \Gamma_{M,(P,Q)} + \varepsilon\Gamma_{S,(P,Q)} \tag{6}$$

$$\Gamma_{M,(P,Q)} = X(1-X)\left(\frac{\Delta M}{M_{(P,Q)}}\right)^2 \tag{7}$$

where $\Delta M = M_P - M_Q$, and $M_{(P,Q)} = (1-X)M_P + XM_Q$, P = Pb, Te, Q = Sn, Se, X = x/(1+x).

$$\Gamma_{S,(P,Q)} = X(1-X)\left(\frac{\Delta r}{r_{(P,Q)}}\right)^2 \tag{8}$$

where $\Delta r = r_P - r_Q$, and $r_{(P,Q)} = (1-X)r_P + Xr_Q$.

And then,

$$\Gamma_{(P,Q)} = \frac{1}{2}\left(\frac{M_{(P,Q)}}{\overline{M}}\right)^2 X(1-X)\left[\left(\frac{\Delta M}{M_{(P,Q)}}\right)^2 + \varepsilon\left(\frac{\Delta r}{r_{(P,Q)}}\right)^2\right] \tag{9}$$

The details of calculation result are shown in Table S3. As shown in Fig. 4 (d), the theoretically calculated lattice thermal conductivity in PbTe−y%SnSe (y = 0–4) based on Callaway model is higher than experimental results at room temperature. The mismatch between theoretically predicted value and measured value indicates some extra contributions to phonon scattering besides point defect. Therefore, in order to explore the structural

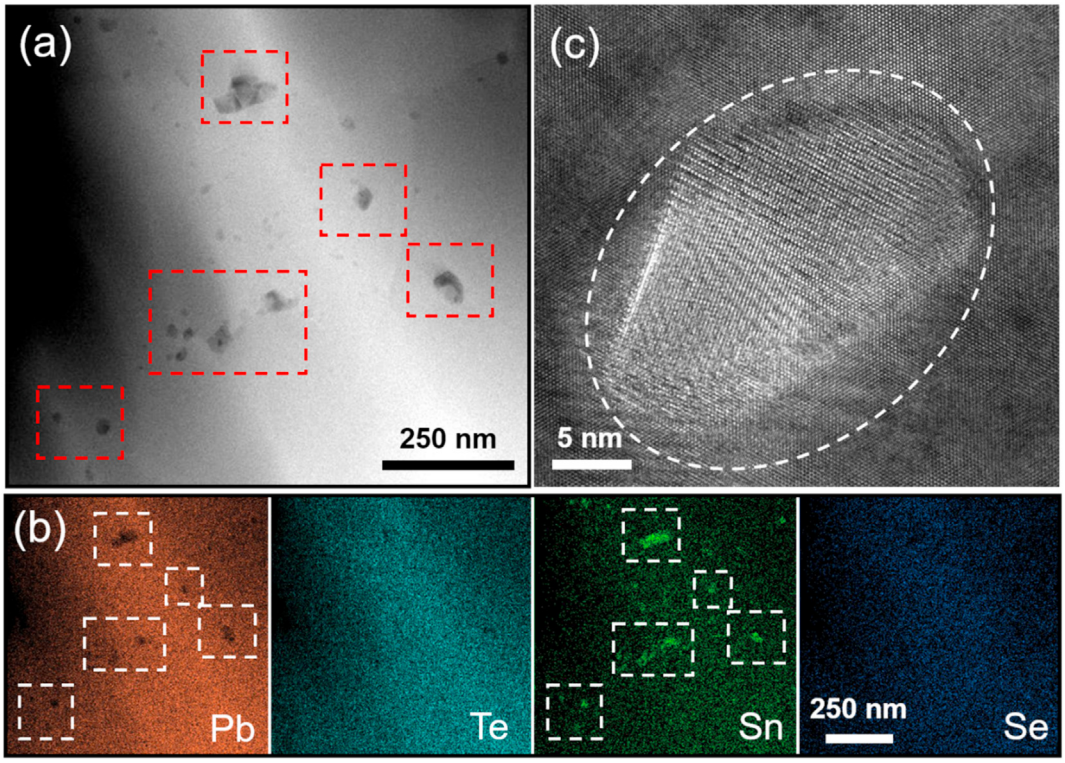

Fig. 5. Microstructure observation in PbTe−2%SnSe: (a) STEM HAADF image of Sn-rich nanoprecipitates; (b) EDS elemental mapping of Pb, Te, Sn, and Se from the selected area in (a); (c) high-magnification TEM image of Sn-rich nanoprecipitates from the selected area in (a).

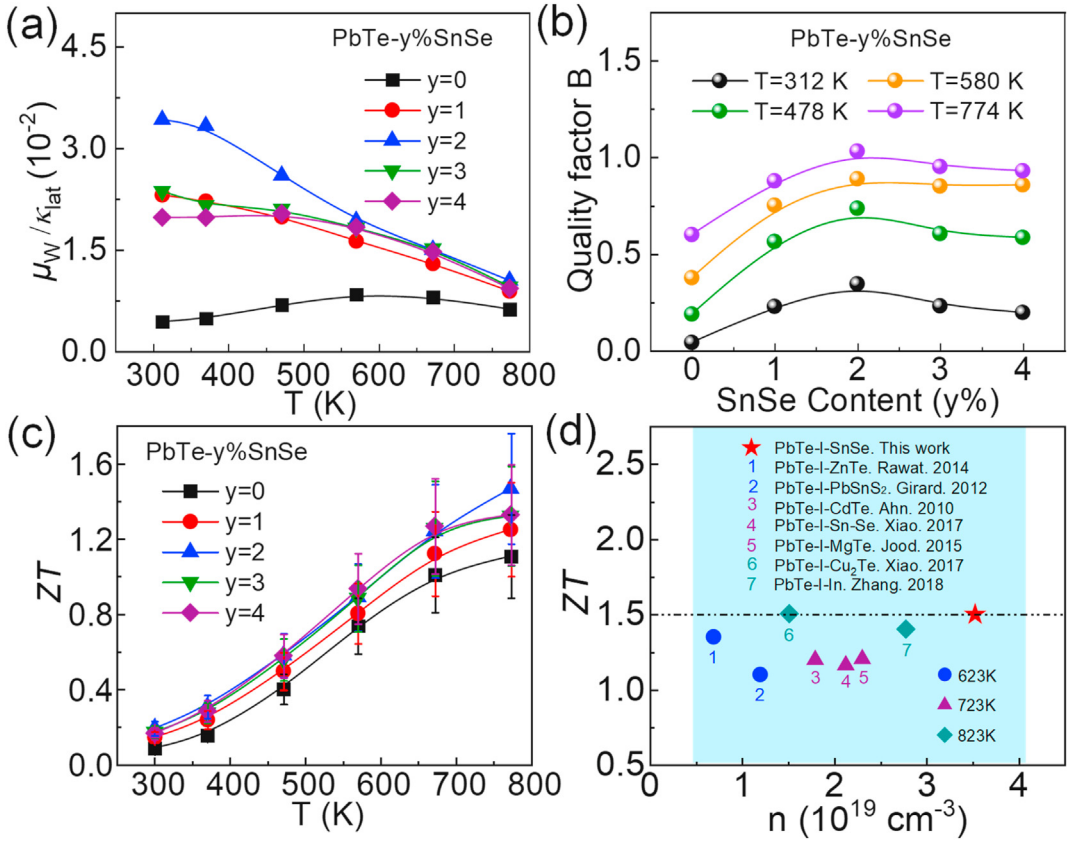

Fig. 6. Thermoelectric performance of PbTe−y%SnSe (y = 0–4): (a) the ratio of weighted mobility to lattice thermal conductivity (μ_w/κ_{lat}) as a function of temperature, the unit of μ_w/κ_{lat} is $cm^2V^{-1}s^{-1}/Wm^{-1}K^{-1}$; (b) quality factor *B*, the unit of *B* is $m^2V^{-1}s^{-1}/Wm^{-1}K^{-1}$; (c) *ZT* value; (d) *ZT* value comparisons with some other high-performance *n*-type PbTe samples: PbTe−I−ZnTe [54], PbTe−I−$PbSnS_2$ [55], PbTe−I−CdTe [56], PbTe−I−Sn−Se [49], PbTe−I−MgTe [57], PbTe−I−Cu_2Te [34], PbTe−I−In [58].

origins of the lowered lattice thermal conductivity in PbTe−y% SnSe (y = 0−4), the microstructure observation is conducted. The STEM HAADF (high angle annular dark field) image of PbTe−2% SnSe sample in Fig. 5(a) shows many nanoprecipitates with size in tens of nanometer. STEM-EDS element mapping proves that Se element is homogeneously dispersed in PbTe−2%SnSe, and these nanoscale precipitates are Sn-rich, Fig. 5(b). High-magnification TEM in Fig. 5(c) shows the crystal structure of precipitates in the dotted box is obviously different from the matrix, which could intensify phonon scattering to reduce lattice thermal conductivity.

Quality factor and *ZT* value in PbTe−y%SnSe (y=0−4). The contribution of SnSe to the thermoelectric performance in PbTe can be evaluated by quality factor *B*, which is defined by following relation [52,53]:

$$B = 9\frac{\mu_W}{\kappa_{lat}}\left(\frac{T}{300}\right)^{5/2} \quad (10)$$

where the μ_W is the weighted mobility, and the temperature-dependent μ_w/κ_{lat} is plotted in Fig. 6(a). After SnSe alloying in PbTe, the μ_w/κ_{lat} of all samples is significantly enhanced. This enhanced μ_w/κ_{lat} value in PbTe−y%SnSe (y = 0−4) means that the imported defects in matrix can intensify phonon scattering while maintain high carrier mobility, successfully realizing synergistic optimization between carrier and phonon transport. Fig. 6(b) shows the calculated *B* value at different temperatures. With increasing SnSe content, the *B* value firstly increases and then decreases, and the peak *B* value can be obtained in PbTe−2%SnSe. Consequently, with successive I doping and SnSe alloying, the *ZT* value in *n*-type PbTe achieves a large enhancement, and the peak *ZT* value increases from ~1.1 in PbTe to ~1.5 in PbTe−2%SnSe, shown in Fig. 6(c). The average *ZT* increases from ~0.63 in PbTe to ~0.82 in PbTe−2%SnSe at 300−773 K, as shown in Fig. S5. Additionally, the heating−cooling cycle measurements for PbTe−2%SnSe demonstrate a good repeatability and thermal stability in Fig. S6. Compared with some other *n*-type PbTe-based materials in Fig. 6(d), PbTe−2%SnSe presents a relatively high *ZT* value.

4. Conclusions

In summary, the electrical and thermal performance in *n*-type PbTe is synergistically optimized by I doping and SnSe alloying. Experiments show that I element is a good donor dopant to tune the carrier density and SnSe alloying can effectively regulated the coupling relations between effective mass and carrier mobility. Meanwhile, the introduction of Sn-rich nanoprecipitates enhances phonon scattering without strongly hindering carrier transport, which effectively suppresses lattice thermal conductivity while maintaining excellent electrical transport properties. After optimizing the electrical and thermal performance, we obtained a significant improved peak *ZT* value of ~1.5 in PbTe−2%SnSe at 773 K. Our results show that maximally balancing the carrier and phonon transport is of great importance to improve thermoelectric properties.

Credit author statement

Wei Liu: data curation, writing-original draft. **Tao Hong**: SEM and TEM data curation. **Shizhi Dong**: formal analysis. **Dongyang Wang**: formal analysis. **Xiang Gao**: SEM and TEM data curation. **Yu Xiao**: formal analysis, project administration, writing-review & editing and funding acquisition. **Li-Dong Zhao**: conceptualization, project administration, supervision, writing-review & editing, funding acquisition.

Declaration of competing interest

The authors declare that they have no known competing financial interests or personal relationships that could have appeared to influence the work reported in this paper.

Acknowledgments

We acknowledge the financial support from the Fundamental Research Funds for the Central Universities (xtr042021007), Top Young Talents Programme of Xi'an Jiaotong University, National Natural Science Foundation of China (52172236), National Science Fund for Distinguished Young Scholars (51925101), and National Postdoctoral Program for Innovative Talents (BX20200028).

Appendix A. Supplementary data

Supplementary data to this article can be found online at https://doi.org/10.1016/j.mtener.2022.100983.

References

[1] X. Shi, L.D. Chen, Thermoelectric materials step up, Nat. Mater. 15 (2016) 691−692, https://doi.org/10.1038/nmat4643.
[2] K.F. Hsu, S. Loo, F. Guo, W. Chen, J.S. Dyck, C. Uher, T. Hogan, E.K. Polychroniadis, M.G. Kanatzidis, Cubic $AgPb_mSbTe_{2+m}$: bulk thermoelectric materials with high figure of merit, Science 303 (2004) 818−821, https://doi.org/10.1126/science.1092963.
[3] W. Liu, J. Hu, S. Zhang, M. Deng, C.G. Han, Y. Liu, New trends, strategies and opportunities in thermoelectric materials: a perspective, Mater. Today Phys. 1 (2017) 50−60, https://doi.org/10.1016/j.mtphys.2017.06.001.
[4] D. Wu, Y. Pei, Z. Wang, H. Wu, L. Huang, L.-D. Zhao, J. He, Significantly enhanced thermoelectric performance in n-type heterogeneous BiAgSeS composites, Adv. Funct. Mater. 24 (2014) 7763−7771, https://doi.org/10.1002/adfm.201402211.
[5] X. Zhang, C. Chang, Y. Zhou, L.D. Zhao, BiCuSeO thermoelectrics: an update on recent progress and perspective, Materials 10 (2017) 198, https://doi.org/10.3390/ma10020198.
[6] X. Su, S. Hao, T.P. Bailey, W. Si, M.G. Kanatzidis, Weak electron phonon coupling and deep level impurity for high thermoelectric performance $Pb_{1-x}Ga_xTe$, Adv. Energy Mater. 8 (2018) 1800659, https://doi.org/10.1002/aenm.201800659.
[7] X. Zhou, Y. Yan, X. Lu, H. Zhu, X. Han, G. Chen, Z. Ren, Routes for high-performance thermoelectric materials, Mater. Today 21 (2018) 974−988, https://doi.org/10.1016/j.mattod.2018.03.039.
[8] Y.-L. Pei, H. Wu, J. Sui, J. Li, D. Berardan, C. Barreteau, L. Pan, N. Dragoe, W.-S. Liu, J. He, L.-D. Zhao, High thermoelectric performance in *n*-type BiAgSeS due to intrinsically low thermal conductivity, Energy Environ. Sci. 6 (2013) 1750−1755, https://doi.org/10.1039/c3ee40879e.
[9] Y. Qiu, Y. Jin, D. Wang, M. Guan, W. He, S. Peng, R. Liu, X. Gao, L.-D. Zhao, Realizing high thermoelectric performance in GeTe through decreasing the phase transition temperature via entropy engineering, J. Mater. Chem. A. 7 (2019) 26393−26401, https://doi.org/10.1039/c9ta10963c.
[10] D.I. B, Jiaqing H, Hui-Qing W, S.N. G, Morphology control of nanostructures: Na-doped PbTe-PbS system, Nano Lett. 12 (2012) 5979−5984, https://doi.org/10.1021/nl303449x.
[11] H. Wu, J. Carrete, Z. Zhang, Y. Qu, X. Shen, W. Zhao, L.-D. Zhao, J. He, Strong enhancement of phonon scattering through nanoscale grains in lead sulfide thermoelectrics, NPG Asia Mater. 6 (2014) e108, https://doi.org/10.1038/am.2014.39.
[12] T.R. Wei, C.F. Wu, L. Fu, J.F. Li, Low-cost and environmentally benign selenides as promising thermoelectric materials, J. Materiomics. 4 (2018) 304−320, https://doi.org/10.1016/j.jmat.2018.07.001.
[13] X. Liu, D. Wang, H. Wu, J. Wang, Y. Zhang, G. Wang, S.J. Pennycook, L.-D. Zhao, Intrinsically low thermal conductivity in BiSbSe3: a promising thermoelectric material with multiple conduction bands, Adv. Funct. Mater. 29 (2019) 1806558, https://doi.org/10.1002/adfm.201806558.
[14] B.-C. Qin, Y. Xiao, Y.-M. Zhou, L.-D. Zhao, Thermoelectric transport properties of Pb-Sn-Te-Se system, Rare Met. 37 (2017) 343−350, https://doi.org/10.1007/s12598-017-0991-9.
[15] Y. Xiao, D. Wang, B. Qin, J. Wang, G. Wang, L.-D. Zhao, Approaching topological insulating states leads to high thermoelectric performance in *n*-type PbTe, J. Am. Chem. Soc. 140 (2018) 13097−13102, https://doi.org/10.1021/jacs.8b09029.
[16] A.J. Strauss, Effect of Pb- and Te-saturation on carrier concentrations in impurity-doped PbTe, J. Electron. Mater. 2 (1973) 553−569, https://doi.org/10.1007/BF02655875.

[17] J. He, S.N. Girard, M.G. Kanatzidis, V.P. Dravid, Microstructure-lattice thermal conductivity correlation in nanostructured $PbTe_{0.7}S_{0.3}$ thermoelectric materials, Adv. Funct. Mater. 20 (2010) 764–772, https://doi.org/10.1002/adfm.200901905.

[18] Y. Pei, A.F. May, G.J. Snyder, Self-tuning the carrier concentration of PbTe/Ag_2Te composites with excess Ag for high thermoelectric performance, Adv. Energy Mater. 1 (2011) 291–296, https://doi.org/10.1002/aenm.201000072.

[19] D. Ginting, C.-C. Lin, L. Rathnam, J.H. Yun, B.-K. Yu, S.-J. Kim, J.-S. Rhyee, High thermoelectric performance due to nano-inclusions and randomly distributed interface potentials in N-type $(PbTe_{0.93-x}Se_{0.07}Cl_x)_{0.93}(PbS)_{0.07}$ composites, J. Mater. Chem. A. 5 (2017) 13535–13543, https://doi.org/10.1039/c7ta02643a.

[20] C. Chang, G. Tan, J. He, M.G. Kanatzidis, L.-D. Zhao, The thermoelectric properties of SnSe continue to surprise: extraordinary electron and phonon transport, Chem. Mater. 30 (2018) 7355–7367, https://doi.org/10.1021/acs.chemmater.8b03732.

[21] S. Yan, Z.C. Zhong, C. Franchini, D. Li, X.Q. Chen, Rocksalt SnS and SnSe: native topological crystalline insulators, Phys. Rev. B 88 (2013) 235122, https://doi.org/10.1103/PhysRevB.88.235122.

[22] D. Ginting, C.-C. Lin, L. Rathnam, G. Kim, J.H. Yun, H.S. So, H. Lee, B.K. Yu, S.J. Kim, K. Ahn, Enhancement of thermoelectric performance in Na-doped $Pb_{0.6}Sn_{0.4}Te_{0.95-x}Se_xS_{0.05}$ via breaking the inversion symmetry, band convergence, and nanostructuring by multiple elements doping, ACS Appl. Mater. Interfaces 10 (2018) 11613–11622, https://doi.org/10.1021/acsami.7b18362.

[23] C. Chang, D. Wang, D. He, W. He, F. Zhu, G. Wang, J. He, L.-D. Zhao, Realizing high-ranged out-of-plane ZTs in N-type SnSe crystals through promoting continuous phase transition, Adv. Energy Mater. 9 (2019) 1901334, https://doi.org/10.1002/aenm.201901334.

[24] J. Shen, X. Zhang, S. Lin, J. Lin, Z. Chen, W. Li, Y. Pei, Vacancy scattering for enhancing the thermoelectric performance of $CuGaTe_2$ solid solutions, J. Mater. Chem. A (2016), https://doi.org/10.1039/C6TA06033A, 10.1039.C1036TA06033A.

[25] Y. Wei, D. Yang, Y. Yan, K. Peng, X. Zhou, Synergistic strategy to enhance the thermoelectric properties of $CoSbS_{1-x}Se_x$ compounds via solid solution, ACS Appl. Mater. Interfaces 9 (2017) 10595–10601, https://doi.org/10.1021/acsami.6b12796.

[26] S. Il Kim, K.H. Lee, H.A. Mun, H.S. Kim, S.W. Hwang, J.W. Roh, D.J. Yang, W.H. Shin, X.S. Li, Y.H. Lee, Dense dislocation arrays embedded in grain boundaries for high-performance bulk thermoelectrics, Science 348 (2015) 109–114, https://doi.org/10.1126/science.aaa4166.

[27] Z. Chen, B. Ge, W. Li, S. Lin, J. Shen, Y. Chang, R. Hanus, G.J. Snyder, Y. Pei, Vacancy-induced dislocations within grains for high-performance PbSe thermoelectrics, Nat. Commun. 8 (2017) 13828, https://doi.org/10.1038/ncomms13828.

[28] G. Tan, F. Shi, S. Hao, L.-D. Zhao, M.G. Kanatzidis, Non-equilibrium processing leads to record high thermoelectric figure of merit in PbTe-SrTe, Nat. Commun. 7 (2016) 12167, https://doi.org/10.1038/ncomms12167.

[29] K. Biswas, J. He, Q. Zhang, G. Wang, C. Uher, V.P. Dravid, M.G. Kanatzidis, Strained endotaxial nanostructures with high thermoelectric figure of merit, Nat. Chem. 3 (2011) 160–166, https://doi.org/10.1038/nchem.955.

[30] K. Biswas, J. He, I.D. Blum, C.I. Wu, T.P. Hogan, D.N. Seidman, V.P. Dravid, M.G. Kanatzidis, High-performance bulk thermoelectrics with all-scale hierarchical architectures, Nature 489 (2012) 414–418, https://doi.org/10.1038/nature11439.

[31] X. Meng, Z. Liu, B. Cui, D. Qin, H. Geng, W. Cai, L. Fu, J. He, Z. Ren, J. Sui, Grain boundary engineering for achieving high thermoelectric performance in *n*-type skutterudites, Adv. Energy Mater. 7 (2017) 1602582, https://doi.org/10.1002/aenm.201602582.

[32] W.-W. Qu, X.-X. Zhang, B.-F. Yuan, L.-D. Zhao, Homologous layered $InFeO_3(ZnO)_m$: new promising abradable seal coating materials, Rare Met. 37 (2017) 79–94, https://doi.org/10.1007/s12598-017-0978-6.

[33] P.F.G. Dalba, EXAFS debye-waller factor and thermal vibrations of crystals, J. Synchrotron Radiat. 4 (1997) 243–255, https://doi.org/10.1107/S0909049597006900.

[34] Y. Xiao, H. Wu, W. Li, M. Yin, Y. Pei, Y. Zhang, L. Fu, Y. Chen, S.J. Pennycook, L. Huang, J. He, L.-D. Zhao, Remarkable roles of Cu to synergistically optimize phonon and carrier transport in *n*-type PbTe-Cu_2Te, J. Am. Chem. Soc. 139 (2017) 18732–18738, https://doi.org/10.1021/jacs.7b11662.

[35] A. Bali, R. Chetty, A. Sharma, G. Rogl, P. Heinrich, S. Suwas, D.K. Misra, P. Rogl, E. Bauer, R.C. Mallik, Thermoelectric properties of In and I doped PbTe, J. Appl. Phys. 120 (2016) 175101, https://doi.org/10.1063/1.4965865.

[36] Y. Pei, J. Lensch-Falk, E.S. Toberer, D.L. Medlin, G.J. Snyder, High thermoelectric performance in PbTe due to large nanoscale Ag_2Te precipitates and La doping, Adv. Funct. Mater. 21 (2011) 241–249, https://doi.org/10.1002/adfm.201000878.

[37] J.R. Sootsman, H. Kong, C. Uher, J.J. D'Angelo, C.I. Wu, T.P. Hogan, T. Caillat, M.G. Kanatzidis, Large enhancements in the thermoelectric power factor of bulk PbTe at high temperature by synergistic nanostructuring, Angew. Chem., Int. Ed. Engl. 47 (2008) 8618–8622, https://doi.org/10.1002/anie.200803934.

[38] Y. Pei, X. Shi, A. Lalonde, H. Wang, L. Chen, G.J. Snyder, Convergence of electronic bands for high performance bulk thermoelectrics, Nature 473 (2011) 66–69, https://doi.org/10.1038/nature09996.

[39] S.Y. Xu, C. Liu, N. Alidoust, M. Neupane, D. Qian, I. Belopolski, J.D. Denlinger, Y.J. Wang, H. Lin, L.A. Wray, Observation of a topological crystalline insulator phase and topological phase transition in $Pb_{1-x}Sn_xTe$, Nat. Commun. 7 (2016) 12505, https://doi.org/10.1038/ncomms12505.

[40] Y. Pei, A.D. Lalonde, H. Wang, G.J. Snyder, Low effective mass leading to high thermoelectric performance, Energy Environ. Sci. 5 (2012) 7963–7969, https://doi.org/10.1039/c2ee21536e.

[41] W. He, D. Wang, J.-F. Dong, Y. Qiu, L. Fu, Y. Feng, Y. Hao, G. Wang, J. Wang, C. Liu, J.-F. Li, J. He, L.-D. Zhao, Remarkable electron and phonon band structures lead to a high thermoelectric performance $ZT > 1$ in earth-abundant and eco-friendly SnS crystals, J. Mater. Chem. A. 6 (2018) 10048–10056, https://doi.org/10.1039/c8ta03150a.

[42] X. Qian, H. Wu, D. Wang, Y. Zhang, J. Wang, G. Wang, L. Zheng, S.J. Pennycook, L.-D. Zhao, Synergistically optimizing interdependent thermoelectric parameters of *n*-type PbSe through alloying CdSe, Energy Environ. Sci. 12 (2019) 1969–1978, https://doi.org/10.1039/c8ee03386b.

[43] E.S. Toberer, A. Zevalkink, G.J. Snyder, Phonon engineering through crystal chemistry, J. Mater. Chem. 21 (2011) 15843–15852, https://doi.org/10.1039/c1jm11754h.

[44] Y. Zhu, Y. Liu, G. Ren, X. Tan, M. Yu, Y.H. Lin, C.W. Nan, A. Marcelli, T. Hu, W. Xu, Lattice dynamics and thermal conductivity in $Cu_2Zn_{1-x}Co_xSnSe_4$, Inorg. Chem. 57 (2018) 6051–6056, https://doi.org/10.1021/acs.inorgchem.8b00569.

[45] G. K, J. F, Efficiency of ab-initio total energy calculations for metals and semiconductors using a plane-wave basis set-ScienceDirect, Comput. Mater. Sci. 6 (1996) 15–50, https://doi.org/10.1016/0927-0256(96)00008-0.

[46] Y. Zhu, Y. Liu, M. Wood, N.Z. Koocher, Y. Liu, L. Liu, T. Hu, J.M. Rondinelli, J. Hong, G.J. Snyder, W. Xu, Synergistically optimizing carrier concentration and decreasing sound velocity in *n*-type $AgInSe_2$ thermoelectrics, Chem. Mater. 31 (2019) 8182–8190, https://doi.org/10.1021/acs.chemmater.9b03011.

[47] C.L. Wan, W. Pan, Q. Xu, Y.X. Qin, M.H. Fang, Effect of point defects on the thermal transport properties of $(La_xGd_{1-x})_2Zr_2O_7$: experiment and theoretical model, Phys. Rev. B 74 (2006) 144109, https://doi.org/10.1103/PhysRevB.74.144109.

[48] G. Tan, F. Shi, H. Sun, L.D. Zhao, C. Uher, V.P. Dravid, M.G. Kanatzidis, SnTe-$AgBiTe_2$ as an efficient thermoelectric material with low thermal conductivity, J. Mater. Chem. A. 2 (2014) 20849–20854, https://doi.org/10.1039/c4ta05530f.

[49] Y. Xiao, W. Li, C. Chang, Y. Chen, L. Huang, J. He, L.-D. Zhao, Synergistically optimizing thermoelectric transport properties of *n*-type PbTe via Se and Sn co-alloying, J. Alloys Compd. 724 (2017) 208–221, https://doi.org/10.1016/j.jallcom.2017.06.296.

[50] R. Gurunathan, R. Hanus, G.J. Snyder, Alloy scattering of phonons, Materials Horizons 7 (2020) 1452–1456, https://doi.org/10.1039/c9mh01990a.

[51] R.J. Korkosz, T.C. Chasapis, S.H. Lo, J.W. Doak, Y.J. Kim, C.I. Wu, E. Hatzikraniotis, T.P. Hogan, D.N. Seidman, C. Wolverton, High ZT in *p*-Type $(PbTe)_{1-2x}(PbSe)_x(PbS)_x$ Thermoelectric Materials, J. Am. Chem. Soc. 136 (2014) 3225–3237, https://doi.org/10.1021/ja4121583.

[52] R.P. Chasmar, R. Stratton, The thermoelectric figure of merit and its relation to thermoelectric generators, Int. J. Electron. 7 (1959) 52–72, https://doi.org/10.1080/00207215908937186.

[53] G. Tan, L.-D. Zhao, M.G. Kanatzidis, Rationally designing high-performance bulk thermoelectric materials, Chem. Rev. 116 (2016) 12123–12149, https://doi.org/10.1021/acs.chemrev.6b00255.

[54] P.K. Rawat, B. Paul, P. Banerji, Exploration of Zn resonance levels and thermoelectric properties in I-doped PbTe with ZnTe nanostructures, ACS Appl. Mater. Interfaces 6 (2014) 3995–4004, https://doi.org/10.1021/am405410e.

[55] S.N. Girard, T.C. Chasapis, J. He, X. Zhou, E. Hatzikraniotis, C. Uher, K.M. Paraskevopoulos, V.P. Dravid, M.G. Kanatzidis, PbTe-$PbSnS_2$ thermoelectric composites: low lattice thermal conductivity from large microstructures, Energy Environ. Sci. 5 (2012) 8716–8725, https://doi.org/10.1039/c2ee22495j.

[56] K. Ahn, M.K. Han, J. He, J. Androulakis, S. Ballikaya, C. Uher, V.P. Dravid, M.G. Kanatzidis, Exploring resonance levels and nanostructuring in the PbTe-CdTe system and enhancement of the thermoelectric figure of merit, J. Am. Chem. Soc. 132 (2010) 5227–5235, https://doi.org/10.1021/ja910762q.

[57] P. Jood, M. Ohta, M. Kunii, X. Hu, H. Nishiate, A. Yamamoto, M.G. Kanatzidis, Enhanced average thermoelectric figure of merit of n-type $PbTe_{1-x}I_x$-MgTe, J. Mater. Chem. C. 3 (2015) 10401–10408, https://doi.org/10.1039/c5tc01652e.

[58] S.Q.Z. Qian, W. Xinyu, S. Jingying, Deep defect level engineering: a strategy of optimizing the carrier concentration for high thermoelectric performance, Energy Environ. Sci. 11 (2018) 933–940, https://doi.org/10.1039/c8ee00112j.